FPGA-Based Dual-Pulse Anti-Interference Lidar System Using Digital Chaotic Pulse Position Modulation

Minghai Yu, Mengyue Shi, Weisheng Hu, *Member, IEEE*, and Lilin Yi, *Member, IEEE*

***Abstract*— We investigated an FPGA-based dual-pulse anti-interference light detection and ranging (LiDAR) system with digital chaotic pulse position modulation (DCPPM). The dual-pulse signal is a periodic pulse pair, in which the first pulse is a periodic pulse, and the second pulse based on DCPPM is a pulse with a random time interval from the first pulse in each period. The real-time generation and detection of the position-modulated dual-pulse are realized by a field-programmable gate array (FPGA). The DCPPM-based dual-pulse lidar system integrates the characteristics of anti-interference, high pulse peak power, and fast measurement. In this letter, the repetition frequency of the dual-pulse signal is 100kHz. There is an initial time interval of 128ns between dual pulses, the step number of random time interval between dual pulses is 0∼255, and the step accuracy is 6.4ns. Under a 1.25GSa/s sampling rate of the analog to digital converter (ADC), an accuracy within ±6cm has been obtained. Finally, under 100kHz periodic pulse interference and 100kHz DCPPM-based dual-pulse interference, the probability of correct detection has been counted every 250 measurements (up to 2000 times). The two correct detection probabilities with average values above 99% have been obtained, which are respectively 99.29% and 99.68%. The good anti-interference performance of the proposed lidar system has been verified.**

***Index Terms*— Real-time, anti-interference, fast measurement.**

I. Introduction

With the rapid development of intelligent technology, light detection and ranging (lidar) plays an important role in autonomous cars, drones, robots, augmented and virtual reality [1]–[5]. For most lidar systems, the time-of-flight of the echo signal relative to the emitted periodic pulse signal is measured to calculate the distance information. The use of high-frequency narrow pulses can obtain high peak power to gain better signal-to-noise ratios (SNRs) and improve the detection ranges [6]. However, the periodicity and regularity of the pulses emitted by conventional pulsed lidars can often cause range ambiguity and make them vulnerable to interference and jamming [7], [8], the reception of unspecific signals from other lidars and light sources will produce ghost images or result in failure of detections.

Manuscript received April 19, 2021; revised May 19, 2021; accepted June 22, 2021. Date of publication June 28, 2021; date of current version July 12, 2021. This work was supported by the Key-Area Research and Development Program of Guangdong Province under Grant 2018B010114002. *(Corresponding author: Lilin Yi.)*

The authors are with the State Key Laboratory of Advanced Optical Communication Systems and Networks, Shanghai Jiao Tong University, Shanghai 200240, China (e-mail: lilinyi@sjtu.edu.cn).

Color versions of one or more figures in this letter are available at https://doi.org/10.1109/LPT.2021.3093109.

Digital Object Identifier 10.1109/LPT.2021.3093109

To solve the problem of interference, random-modulation continuous-wave (RM-CW) lidars have been studied [9]. In an RM-CW lidar, a pseudo-random binary sequence (PRBS) is modulated on a CW laser through an external intensity modulator, and the distance of the target is calculated by correlating a reflected waveform with a time-delayed reference waveform [10]. The unambiguous range is determined by the time duration of the PRBS pre-designed. The range resolution on the other hand is strongly associated with the width of each bit in the PRBS, which in practice is determined by the electronic devices and the modulation speed of the modulator used. By contrast, optical chaos is aperiodic and unpredictable [11]–[14]. Chaotic lidars provide a long unambiguous range and excellent anti-interference performance [15]. Moreover, optical chaos based on nonlinear dynamics of semiconductor lasers can easily be generated through optical injection and/or feedback without any expensive high-speed signal generator or external modulator [16]–[19]. However, compared to the conventional pulsed lidars, the main problem of both the RM-CW lidars and chaotic lidar is that the low pulse peak power limits the SNRs therefore the ranging distance.

In addition to the above two methods of random intensity modulation of continuous waves to resist interference, there is also the method of chaotic pulse position modulation. The CPPM signal consists of a pulse sequence, all pulses have the same pulse width and amplitude, and the time interval between pulses changes according to the chaotic law [20]. The signal combines the characteristics of chaos and pulse signals, which not only has good anti-interference ability of chaotic signals but also guarantees the high peak power of the pulse lidar. There are currently two kinds of CPPM-based lidar according to the method of signal processing. One is similar to the modulated CW lidars, the reflected waveform is correlated with a time-delayed reference waveform to obtain the distance [21]. The second is the time-correlated single-photon counting (TCSPC) lidar which is similar to the pulsed lidars [22], the flight time of the echo pulse signal relative to the emitted pulse signal is calculated to obtain the distance. Since the position of the emitted signal in each period is random, measurement is performed in a large number of periods for histogram statistics. Finally, the echo of the pulse signal emitted by itself will be recorded in a fixed position, and the interference will be distributed in various positions, forming a background noise level. The above-mentioned correlation calculation method of CW lidars needs a long time to store, shift, multiply and accumulate, and the TCSPC of pulsed

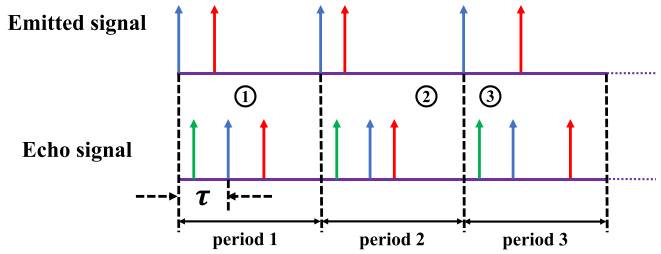

Fig. 1. Emitted signal and echo signal under interference in each period. The blue and red lines represent signal pulses, and the green line represents interference pulses.

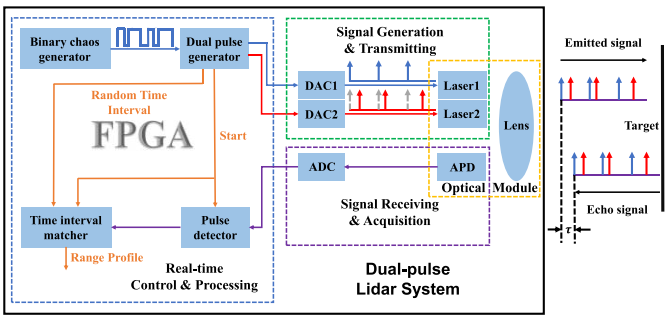

Fig. 2. Experimental setup of DCPPM-based dual-pulse lidar system.

lidars based on CPPM needs a lot of period accumulation. CW lidars based on indirect time-of-flight need to store data and complex mathematical operations, which will consume a lot of storage and computing resources. Pulsed lidars based on direct time-of-flight require very few resources to detect pulses and record pulse positions.

In this letter, a dual-pulse signal based on DCPPM was generated by a field-programmable gate array (FPGA) as the emitted signal. The lidar system can quickly complete a single measurement in one period. For 100kHz dual pulse signal, the initial time interval of the pulse is 128ns, the range of the random time interval is 128ns∼1760ns, and the accuracy is 6.4ns. Under the ADC sampling rate of 1.25GSa/s and the measurement distance range of 19 meters, an accuracy within ±6cm has been obtained. Two correct detection probabilities with average values of 99.29% and 99.68% have been obtained at 100kHz periodic pulse interference and 100kHz DCPPM-based dual-pulse interference under multiple measurements, the good anti-interference performance of the proposed dual-pulse lidar system has been verified.

II. Principles and Experimental Setup

As shown in Fig. 1, the emitted signal of our lidar system is no longer a periodic and regular single pulse, but a pair of pulses with random time intervals in each period. In each period, the first pulse is a periodic pulse, and the random time interval of the second pulse relative to the first pulse is controlled by a binary digital chaotic sequence. When measuring distance, time interval matching on the pulses of the echo signal is performed. The pulse pair that meets the corresponding time interval of the current measurement period is considered to be a reflected signal, and the time-of-flight of the pulse pair is defined as τ. The distance information is $c\tau/2$, where c is the speed of light.

The echo signal in Fig. 1 contains an interference signal. The time interval between the interference pulse and the first pulse of the dual-pulse signal, the time interval between the interference pulse and the second pulse of the dual-pulse signal, and the time interval between the dual pulse signals are defined as delay1, delay2, and delay. Assuming that delay1 = delay or delay2 = delay is satisfied in a certain period, which will result in multiple pulse pairs that meet the time interval matching. Then, the interference will cause misjudgment. However, delay changes randomly in each period, and the interference will not cause misjudgment in the next period or even more periods until delay1 = delay or delay2 = delay is satisfied again.

Figure 2 shows the experimental setup of the proposed dual-pulse lidar system. The FPGA generates electric dual-pulse signal, and drives the lasers to emit optical dual-pulse signal through the digital to analog converter (DAC) output. The target of distance measurement is a standard plate with a reflectivity of 60%. The echo signal is detected by the Avalanche Photo Diode (APD), and the optical signal is converted into an electrical signal. The electrical signal is collected by ADC and processed by FPGA.

A multifunctional development board equipped with one FPGA chip (Stratix V: 5SGXEA7K2F40C2), two pieces of 5GSPs high-speed ADC (EV8AQ160), and two pieces of 2.5GSPs high-speed DAC (AD9739ABBCZ) is used. All digital signal processing is completed on the development board.

Two lasers with a repetition frequency of 100kHz, a duty cycle of 0.1%, and a peak power of 100W are used to generate optical dual-pulse signal. An APD with a bandwidth of 200MHz is used to detect echo signal. The laser, APD and optical lens are packaged into an optical module. The position of each device in the module is determined by the optical path design, which can ensure a good transmitting and receiving effect.

In the binary chaos generator, the logistic mapping is applied to generate digital chaos and binary quantization.

The logistic mapping model is as follows

$$x_{n+1} = \mu x_n \cdot (1 - x_n) \quad n = 1, 2, 3, \ldots \tag{1}$$

In order to ensure that the logistic mapping is in a chaotic state, the value range of the parameters is as follows

$$3.569946 \cdots < \mu \leq 4, \quad x_n \in (0, 1) \tag{2}$$

In this design, in order to facilitate FPGA operations and ensure that digital chaos has good randomness, the selected parameter and initial value are

$$\mu = 4, \quad x_1 = 0.875 \tag{3}$$

The mean value of logistic map is 0.5, which is used as a criterion to quantify the generated sequence into binary chaos

$$x_n = \begin{cases} 1 & 0.5 < x_n < 1 \\ 0 & 0 < x_n \leq 0.5 \end{cases} \tag{4}$$

To ensure that the result of the operation does not deviate from the chaotic state, in FPGA design, the data length is

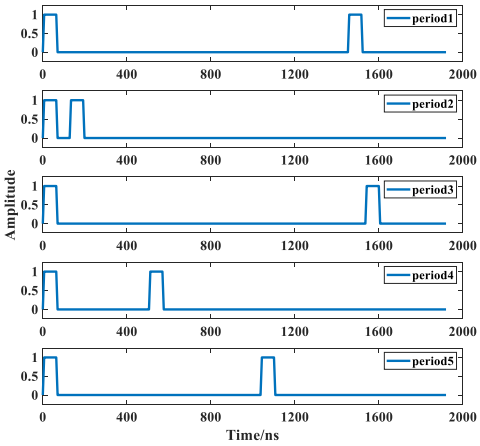

Fig. 3. Electric dual-pulse signal in five different periods. Since the position of the second pulse varies from 128ns to 1760ns, the drive signal is only displayed in 0 to 2us.

selected as 64 bits, in which the highest bit represents the integer part, and the lower 63 bits represent the decimal part. The clock of the binary chaos generator is 156.25M.

The dual pulse generator generates dual pulses with random time intervals in each period. Binary chaos enters the dual pulse generator as input, and the clock used by this module is the same 156.25M clock as the binary chaos generator. 8-bit binary chaos is selected to form the corresponding binary number, which is used as the step number corresponding to the random time interval of the next period. The pulse width of the laser drive signal generated by the FPGA is 64 ns, and the initial time interval between dual pulses is 128 ns to avoid overlapping of optical dual pulses. The optical path difference between the dual lasers is calibrated to ensure that the time interval between the optical dual pulses is equal to the electrical time interval. Fig. 3 shows the electric dual-pulse signal in five different periods.

For the Gaussian pulse emitted by our laser, the position corresponding to the maximum value or the position corresponding to the middle point of the pulse is used to represent the position of the pulse. However, the maximum value is easily affected by noise in the real situation. In this letter, the position of the middle point of the pulse is regarded as the pulse position. When the signal distortion is not particularly serious, there is a relatively small measurement error.

In the pulse detector we can set an appropriate threshold. For pulse signals, there will be a continuous sampling value greater than the threshold, but random noise signals will not have such characteristics. Set an appropriate width value according to the pulse width of the lasers and the sampling rate. Only when the continuous sampling value is greater than the threshold and the number of points is greater than the width value, it will be judged as a pulse and output the pulse position.

Figure 4 shows the pulse position detection of the echo signal under different attenuations, where $\boldsymbol{\alpha}$ is the attenuation coefficient, **Th** is the detection threshold, and **pos** is the detected pulse position. The threshold value set according to the noise floor of the system is 50mV. The pulse width of the laser will be widened after APD detection, but the basic effective width remains about 10ns. The attenuation of the signal at different distances will result in inconsistent pulse

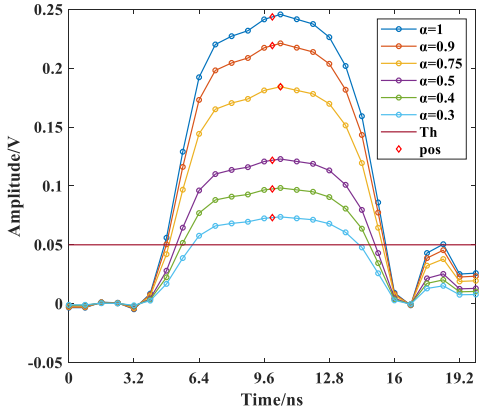

Fig. 4. Pulse position detection of the echo signal under different attenuations.

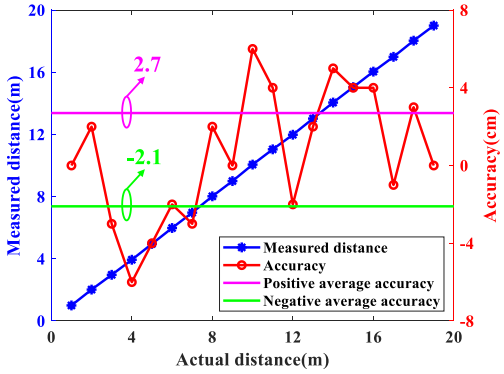

Fig. 5. Measured distance and accuracy at each actual distance.

widths greater than the threshold. Under the condition of ADC sampling rate of 1.25GSa/s, the width value is set to 8 sampling points, that is, pulses with a width greater than 6.4ns above the threshold are regarded as valid signal pulses. It can be seen from Fig. 4 that the deviation of the pulse position we detected under different attenuation is half the sampling point, and the corresponding distance is 6cm.

The random time interval of the dual pulse signal in the pulse generator is input to the time interval matcher as a matching condition for each period (10us), which is the 'Random Time Interval' shown in Fig. 2. The time interval matcher stores the pulse positions detected by the pulse detector and records the number of pulses, and then performs a pairwise match. According to the deviation of the pulse detector, the matching condition is the random time interval plus or minus the time of one sampling point. If there is no pair of pulses that meet the condition after all pulses are matched, the output distance information is 0cm. Otherwise, output the distance information corresponding to the last pair of pulses.

The digital signal control and processing parts are synchronized through the same reference zero point, which is the 'Start' shown in Fig. 2. At the last clock of each period, the initialization required to enter the next period is performed.

III. Ranging and Anti-Interference Results

We conduct interference-free ranging experiments every 1 meter within a distance of 1∼19 meters.

The distance measurement results are shown in the Fig. 5, and the accuracy is within ±6cm. A positive average accuracy

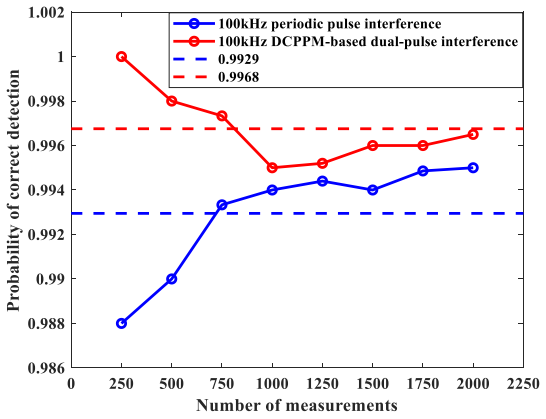

Fig. 6. Probability of correct detection under two kinds of interference.

of 2.7cm and a negative average accuracy of −2.1cm have been obtained. This centimeter-level accuracy meets the needs of autonomous driving scenarios.

In order to test the anti-interference performance of the proposed lidar system, two interference signals were selected for testing. The first is 100kHz periodic pulse interference, and the second is 100kHz dual-pulse interference based on DCPPM. For the second type of interference, its generation is the same as the emitted signal. The only difference is that the initial value of chaos for pulse position modulation is 0.625. Under the two kinds of interference, the correct detection probability is counted every 250 measurements, up to 2000 times.

The anti-interference results are shown in the Fig. 6. Under 100kHz periodic pulse interference, since only the time interval of signal changes randomly, the probability of correct detection may be small at the beginning. However, with the increase of the number of measurements, the probability increases gradually. Finally, the average correct detection probability is 99.29%. For 100kHz DCPPM-based dual-pulse interference, the time interval of the interference is also randomly changing, which may lead to a higher probability of correct detection at the beginning. With the increase of the number of measurements, the influence of interference is gradually revealed. Finally, the average correct detection probability tends to 99.68%. Due to the strong randomness of the time interval, the result of a certain statistics is relatively random, which does not explain any problems, but the average value of multiple statistics can well show the anti-interference ability.

IV. Conclusion

In this letter, we have shown an FPGA-based dual-pulse anti-interference lidar system with digital chaotic pulse position modulation and the step number of random time interval between dual pulses is 0∼255. Under the ADC sampling rate of 1.25GSa/s and the measurement distance range of 19 meters, an accuracy within ±6cm has been obtained. Under 100kHz periodic pulse interference and 100kHz DCPPM-based dual-pulse interference, two correct detection probabilities with average values above 99% have been obtained, which are respectively 99.29% and 99.68%. The good anti-interference performance of the proposed lidar system has been verified. In the measurement process with a large number of points, the misjudgment point caused by interference can be regarded as burrs in the overall measurement results and thus can be eliminated. If the number of random time intervals is increased, the anti-interference performance will be further improved. Besides, with the increase of the ADC sampling rate, the measurement accuracy can also be improved. We believe the proposed anti-interference lidar can find applications such as in the autonomous cars.

References

[1] B. Schwarz, "LIDAR: Mapping the world in 3D," *Nature Photon.*, vol. 4, no. 7, pp. 429–430, 2010.
[2] Q. Li, L. Chen, M. Li, S.-L. Shaw, and A. Nuchter, "A sensor-fusion drivable-region and lane-detection system for autonomous vehicle navigation in challenging road scenarios," *IEEE Trans. Veh. Technol.*, vol. 63, no. 2, pp. 540–555, Feb. 2014.
[3] J. McCormack, J. Prine, B. Trowbridge, A. C. Rodriguez, and R. Integlia, "2D LIDAR as a distributed interaction tool for virtual and augmented reality video games," in *Proc. IEEE Games Entertainment Media Conf. (GEM)*, Oct. 2015, pp. 1–5.
[4] P. Dong and Q. Chen, *LiDAR Remote Sensing and Applications*. Boca Raton, FL, USA: CRC Press, 2017.
[5] Z. Sun, G. Bebis, and R. Miller, "On-road vehicle detection: A review," *IEEE Trans. Pattern Anal. Mach. Intell.*, vol. 28, no. 5, pp. 694–711, May 2006.
[6] M.-C. Amann, T. Bosch, M. Lescure, R. Myllyla, and M. Rioux, "Laser ranging: A critical review of usual techniques for distance measurement," *Opt. Eng.*, vol. 40, no. 1, pp. 10–19, 2001.
[7] G. Kim, J. Eom, and Y. Park, "Investigation on the occurrence of mutual interference between pulsed terrestrial LiDAR scanners," in *Proc. IEEE Intell. Vehicles Symp. (IV)*, Jun. 2015, pp. 437–442.
[8] J. Petit, B. Stottelaar, M. Feiri, and F. Kargl, "Remote attacks on automated vehicles sensors: Experiments on camera and LiDAR," *Black Hat Eur.*, vol. 11, p. 995, Nov. 2015.
[9] X. Ai, R. Nock, N. Dahnoun, and J. G. Rarity, "High resolution random-modulation CW LiDAR," *Appl. Opt.*, vol. 50, no. 22, pp. 4478–4488, 2011.
[10] N. Takeuchi, N. Sugimoto, H. Baba, and K. Sakurai, "Random modulation CW LiDAR," *Appl. Opt.*, vol. 22, no. 9, pp. 1382–1386, 1983.
[11] F.-Y. Lin and J.-M. Liu, "Chaotic LiDAR," *IEEE J. Sel. Topics Quantum Electron.*, vol. 10, no. 5, pp. 991–997, Oct. 2004.
[12] W. T. Wu, Y. H. Liao, and F. Y. Lin, "Noise suppressions in synchronized chaos LiDARs," *Opt. Exp.*, vol. 18, no. 25, pp. 26155–26162, 2010.
[13] C.-H. Cheng, Y.-C. Chen, and F.-Y. Lin, "Generation of uncorrelated multichannel chaos by electrical heterodyning for multiple-input–multiple-output chaos radar application," *IEEE Photon. J.*, vol. 8, no. 1, pp. 1–14, Feb. 2016.
[14] F.-Y. Lin and J.-M. Liu, "Chaotic radar using nonlinear laser dynamics," *IEEE J. Quantum Electron.*, vol. 40, no. 6, pp. 815–820, Jun. 2004.
[15] C.-H. Cheng, C.-Y. Chen, J.-D. Chen, D.-K. Pan, K.-T. Ting, and F.-Y. Lin, "3D pulsed chaos LiDAR system," *Opt. Exp.*, vol. 26, no. 9, p. 12230, Apr. 2018.
[16] F.-Y. Lin, Y.-K. Chao, and T.-C. Wu, "Effective bandwidths of broadband chaotic signals," *IEEE J. Quantum Electron.*, vol. 48, no. 8, pp. 1010–1014, Aug. 2012.
[17] J. Mork, B. Tromborg, and J. Mark, "Chaos in semiconductor lasers with optical feedback: Theory and experiment," *IEEE J. Quantum Electron.*, vol. 28, no. 1, pp. 93–108, 1992.
[18] Y.-H. Liao and F.-Y. Lin, "Dynamical characteristics and their applications of semiconductor lasers subject to both optical injection and optical feedback," *Opt. Exp.*, vol. 21, no. 20, pp. 23568–23578, Sep. 2013.
[19] A. Uchida, T. Heil, Y. Liu, P. Davis, and T. Aida, "High-frequency broadband signal generation using a semiconductor laser with a chaotic optical injection," *IEEE J. Quantum Electron.*, vol. 39, no. 11, pp. 1462–1467, Nov. 2003.
[20] N. Rulkov and L. Larson, "Chaotic pulse position modulation: A robust method of communicating with chaos," *Commun. Lett.*, vol. 4, no. 4, pp. 128–130, 2000.
[21] K. Zhou *et al.*, "Design and implementation of CPPM microwave source for UWB radar system," *Chin. J. Electron Devices*, vol. 38, no. 5, pp. 1042–1047, Oct. 2015.
[22] J. Hao *et al.*, "Ultra-low power anti-crosstalk collision avoidance light detection and ranging using chaotic pulse position modulation approach," *Chin. Phys. B*, vol. 25, no. 7, 2016, Art. no. 074207.